Soft Printable Robots With Flexible Metal Endoskeleton

Chao-Yu Chen, Benjamin Wee Keong Ang, Yangfan Li, Jun Liu, *Member, IEEE*, Zhuangjian Liu, and Chen-Hua Yeow, *Member, IEEE*

***Abstract*—Recent advancements in soft robotics have seen the rapid development of soft grippers for industrial pick-and-place applications. They are, however, ill-suited to bear heavy loads due to their compliant nature. Paradoxically, researchers have sought to increase the stiffness of soft grippers to improve load-bearing capabilities. Unfortunately, contemporary soft actuators with variable stiffness are fabricated using manual processes and their performance is subject to an individual's mastery. They are therefore not reliable for long-term industrial use. In this article, we present our work on a 3-D-printed metal-endoskeleton-reinforced actuator (MERA) for industrial pick-and-place applications. We also highlight the fabrication processes needed to recreate it repetitively. Using stainless steel splints (SSS), we demonstrate that MERA is able to modulate its stiffness at selective junctures for stable and effective grasping. We also describe our design rationale with a qualitative mathematical model and validate its performance quantitatively using a finite element model, which is further investigated in the following fatigue test. In our experiments, the MERA equipped with SSS is able to output a peak tip force of 8 N, which is a 291% increase compared to the one without metallic reinforcement. In addition, an increase of 76.5% in gripping load and a maximum holding force per actuator of 13.8 N are realized through the stiffness tuning of a MERA-Gripper. Despite significantly improving load-bearing capabilities, the actuator manages to retain an overall low profile with a weight of 82 g. Finally, we adapted the MERA into a reconfigurable gripper and tested its grasping capabilities on objects of various shapes, sizes, and weights.**

***Index Terms*—3-D printing, buckling-restrain, finite element analysis, soft pneumatic actuator, variable stiffness.**

I. Introduction

TRADITIONAL robotic grippers typically consist of rigid joints and links [1] driven by a combination of actuators and motors. They are well-researched and are considered the cornerstone of modern day robotic manipulators. Owing to their structural rigidity and highly precise control schemes, these grippers possess load-bearing capabilities with high repeatability [2]. They are, thus, well suited for augmenting robotic automation of industrial processes. However, advanced grasping that involves handling a variety of objects is not feasible with the same gripper. High precision and repeatability are achievable only because traditional manipulators are programmed to grasp a specific item type with a narrow definition. Industrial production, on the other hand, is often multiphasic and involves an assembly line that comprises different components. Therefore, to simplify automation and controls, flexible or reconfigurable grippers are preferred [3], [4], since traditional robotic end effectors lack the adaptability to accomplish different manipulation tasks. More recently, the rapid development of soft robotics has precipitated research initiatives that are aimed at tackling challenging manipulation tasks. One of which involves improving gripper environmental adaptability using soft grippers. Research interest in soft grippers stems from their intrinsic soft nature, which confers a number of advantages over contemporary rigid-body grippers. Among these, notable characteristics include better mechanical compliance with the workspace and the ability to achieve complex yet controlled deformations over a wide spectrum of length scales [5], [6], [7], [8]. They possess high degrees of freedom, which enable them to achieve stable grasping by conforming to objects of different shapes and sizes.

Soft grippers come in numerous designs, which can be categorized into two broad classes—fingered and nonfingered. Finger-type grippers may range from anywhere between two fingers to anthropomorphic hands and tendrils [8], [9], [10] that strive to enhance dexterity and stability during grasping. These bioinspired end-effectors function by bending or enveloping the finger elements around an object while simultaneously applying contact forces on its surface, much like how a human hand grasps items stably. Nonfingered designs span across a wide variety of mechanisms, such as jamming and microfibers adhesion [11]. Universal gripper, as a subset of the nonfingered designs, gets its name from its inherent nature of adaptivity toward different gripping poses and object orientations. For all universal grippers, granular jamming is a common technique that [12] utilizes pressure modulation of grain-filled elastomeric pockets to reversibly transit between fluidlike and rigid states. In the fluid state, the end-effector adapts to the exterior surface of an object upon contact. Subsequently, applying a vacuum source causes the gripper to harden and grasp the object rigidly. This mechanism is

Manuscript received 18 July 2023; revised 24 November 2023 and 13 March 2024; accepted 2 April 2024. Date of publication 22 April 2024; date of current version 17 May 2024. This paper was recommended for publication by Associate Editor H. Zhao and Editor M. Yim upon evaluation of the reviewers' comments. This work was supported by the A*STAR Industry Alignment Fund – Prepositioning under GrantA20H8A0241. *(Corresponding author: Chao-Yu Chen.)*

Chao-Yu Chen, Benjamin Wee Keong Ang, and Chen-Hua Yeow are with the Biomedical Engineering, National University of Singapore, Singapore 117608 (e-mail: biecc@nus.edu.sg; angwkb@nus.edu.sg; rayeow@nus.edu.sg).

Yangfan Li, Jun Liu, and Zhuangjian Liu are with the Institute of High Performance Computing, Agency for Science, Technology and Research, Singapore 138632 (e-mail: li_yangfan@ihpc.a-star.edu.sg; liuj@ihpc.a-star.edu.sg; liuzj@ihpc.a-star.edu.sg).

This article has supplementary downloadable material available at https://doi.org/10.1109/TRO.2024.3392162, provided by the authors.

Digital Object Identifier 10.1109/TRO.2024.3392162

known as jamming, and its shape adaptation is passive, meaning the process is entirely autonomous [13]. Other research groups have also reported success with alternative forms of nonfingered grippers [14], [15], [16], [17] that are able to grasp a large variety of objects with different shapes and sizes.

Despite having these advantages over traditional manipulators, a few hurdles remain before soft grippers can be deployed in industrial settings at scale. To date, soft grippers are not known for their load-bearing capabilities, primarily because their flexible and low stiffness nature does not provide adequate structural rigidity [8], [9], [10], [18]. Object manipulation is hence limited to those with lower mass like in surgical procedures [19], [20] and some pick and place applications [16], [21], [22], [23] albeit not restricted by neither size nor dimension. Research groups have therefore attempted to marry the benefits of both soft and rigid gripper technologies by melding them into hybrid grippers. Making use of variable stiffness structures, hybrid grippers are able to modulate and control their stiffness, which confers strength or flexibility when needed. For example, Li et al. [24] and Hu et al. [25] applied negative pneumatic pressure to compress particles embedded in the gripper to increase its stiffness and load-bearing capability. With optimized geometry, both actuators with variable stiffness properties can generate about 8 N of force per finger. On the other hand, Hoang et al. [26] used high temperatures to stimulate the transition between a conformable, rubbery state to a stiff glassy state that can achieve high-force grasping. Their soft helical gripper is able to attain 3.8 N and 8 of peak holding forces for horizontal and vertical pulling, respectively. However, to achieve these forces, the helical fabric has to wrap at least one full circumference around the object for a secure hold. Aside from actuation modes, Zhou et al. [27] also demonstrated the use of variable stiffness structures, in the form of deformable phalanges, to enhance contact interactions between the gripper and object while retaining high durability toward blunt forces and sharp objects. The finger actuator has a peak finger force of 6.7 N on a smooth surface and 9.7 N on a spiky one. It was adapted into a three-fingered actuator that can pick up a 1.5 kg durian.

In addition, the fabrication of most contemporary soft grippers requires multiple processes that are typically done by hand [16], [19], [20], [23], [24], [25], [26], [27]. Unfortunately, the outcome of manual processes is highly dependent on one's experience and mastery, which curtails scalability and consistency in actuator performance. In some instances, complex gripper designs necessitate the combination of multiple inhomogeneous materials [19], [20], while others [23] may be physically fused from separate casts. In addition, metallic materials have been introduced into soft actuators before to confer their variable stiffness properties. One study by Henke et al. [28] showed the use of shape memory alloy wires to create a simple variable flexural stiffness beam. Their prototype sees a maximum stiffness change by a factor of 60 to increase load capacity. While their recorded stiffness change is impressive, evidence of the flexural beam withstanding an actual load is lacking. Cooling the shape memory alloy also takes 200 s to reach thermal equilibrium, making it ill-suited for any fast-moving gripping applications. Another work by Hao et al. [29] involved the use of low-melting point alloys embedded into a soft robotic gripper. When heated above a threshold, the alloy transits to a liquid state. It is reportedly able to withstand 780 g of load and 12 N of pull-off force. Nonetheless, much like shape memory alloys, even with an 8 A current supplied to the low melting point alloy, the heating process takes over 30 s, which is too long for gripping applications. While these studies demonstrated novel uses of embedded metallic alloys, functionality as a gripper has been lacking. The durability of the gripper is therefore determined by how well dissimilar constituents are joined since interfaces are usually points of failure and fatigue. Variation in other aspects of gripper performance is also to be expected when crucial strain-limiting components are embedded imprecisely in some of these grippers [30], [31]. 3-D printing has hence emerged as a viable fabrication technique that can produce soft actuators with consistent performance [32], [33], [34], [35]. Unlike manual processes, 3-D printing is fully automated and independent of mastery, which eliminates the chances of human error. Designs of 3-D printed actuators are also not as limited and material composites can be extruded using multimaterial printing to confer unique sensing capabilities [36], [37].

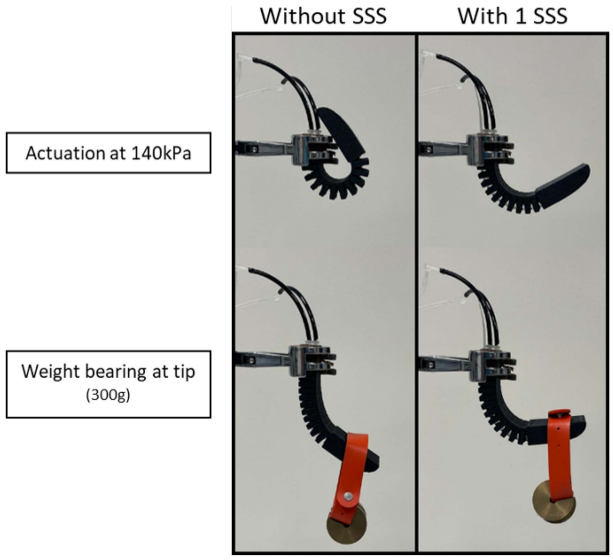

Fig. 1. With the reinforcement of the SSS, the MERA proposed in this research could possess a higher stiffness that enables it to handle the same payload of 300 g more stably.

In light of these aforementioned issues with existing soft grippers, a hybrid 3-D-printed soft pneumatic actuator is proposed (see Fig. 1). The actuator is able to modulate its stiffness between flexible and rigid states through pressure regulation of its pneumatic chambers. The hybrid actuator has a nonlinear behavior, which necessitates the use of finite element analysis to validate its design rationale. To demonstrate the effectiveness of stiffness tuning toward enhancing grasping, a three-fingered gripper is also fabricated to illustrate its ability to carry a variety of loads.

The rest of this article is organized as follows. Section II details the design rationale of the metal-endoskeleton-reinforced

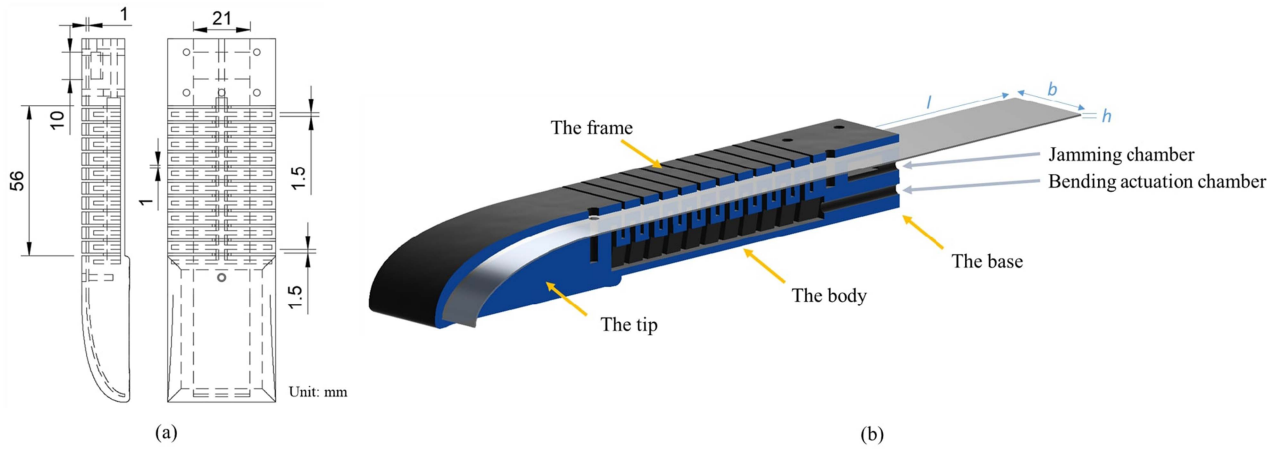

Fig. 2. (a) Internal dimensions of the variable stiffness actuator. (b) Schematic of the components within the actuator.

actuator (MERA). Section III illustrates the finite element analysis of force output from the actuator and compares it with experimental results. Section IV explains the experimental setups and corresponding results under different given input parameters. Section V describes the incorporation of the hybrid actuator into a three-fingered gripper and highlights its advantages in pick-and-place applications. Discussions are presented in Section VI. Finally, Section VII concludes this article.

II. Design Rationale

Soft robotic actuators have the inherent nature of compliance and adaptiveness. However, external impact or collision may cause undesired deformation and lead to grasp instability. On the other hand, a human finger can maintain its grasp on an object by retaining rigidity in the fingers to withstand disturbance. Mimicking the variable stiffness characteristics of a human finger, stiffness can be tuned in robot fingers by programming various stimulus-response reactions. Previous works involving variable stiffness mechanisms include an embedded layer of thermally activated shape memory polymer [38], an enclosed chamber of granular particles responding to negative pressure [25]; and a self-locking mechanism attached at the side of the finger actuator [39]. Nevertheless, the structure of the sensor presents a tradeoff between performance (i.e., increase in stiffness or latency) and bulkiness. In contrast, the MERA designed here is small in size and has low latency.

The MERA consists of three main components—a base, a body, and a fingertip [see Fig. 2(b)]. The length, width, and thickness of the inserted stainless steel splint (SSS) are denoted by l, b, and h, respectively, and $h << b < l$. The base of the MERA hosts the air inlets to two internal pneumatic chambers—a jamming chamber and a bending actuation chamber with multiple bellows. Upon pressurization, the jamming chamber exerts a normal force on the metal strap to generate high friction. The bending actuation chamber then makes up the body, which is seamlessly joined to the tip. In addition, a frame is designed on top of each bellow to house the SSS and minimize buckling [see Fig. 2(b)]. Notably, the jamming channel of the proposed MERA is only 1 mm thin [see Fig. 2(a)] to provide sufficient space for an ideally smooth prismatic joint. If the channel for the SSS is too wide, the effect of buckling restraining would be compromised, due to the lack of constraints on lateral movements. Conversely, if the channel is too thin, the stiffening effect of friction force would impair the bending performance of MERA.

A. Stiffness Tuning

Buckling is defined as the failure of a structure due to high compressive stresses, such as the plate buckling of a thin shell in a pipe or the torsional buckling of an I-beam. However, in this study, we proposed a design to exploit the buckling of a thin plate to tune the overall stiffness of an actuator, as illustrated at the right of Fig. 3. While buckling is a simple physical concept, modeling of a constrained Euler buckling is complex and is sorted using several categorizations [40]. Therefore, finite element analysis is often the primary methodology adopted to elucidate postbuckling response [41]. Nonetheless, mathematicians have been building numerical models to describe elastic plates with buckling and contact boundaries for the past few decades [42]

$$P_{cr} = \frac{\pi^2 E b h^3}{12 L_e} \propto \frac{E_{\text{eff}}}{L_e}. \tag{1}$$

Here, we recognize any two adjacent bellows as an independent jamming unit. Therefore, assuming the deflection of the metal strap within a jamming unit is small and the inflection point is fixed at both ends, we can use (1) to describe the critical load of each jamming unit using the Euler buckling formula, where P_{cr} is the critical load, E indicates the Young's modulus of the material, b refers to the width of the SSS, h refers to the thickness of the SSS, and L_e represents the effective length. Considering that the proposed design incorporates channels and holes, it is essential to employ an effective Young's modulus as a replacement for the term E in (1), alongside the necessary correction of L_e at (2). The influence of the gap distance on the overall stiffness of the finger can be elucidated through the application of homogenization theory [43], wherein the

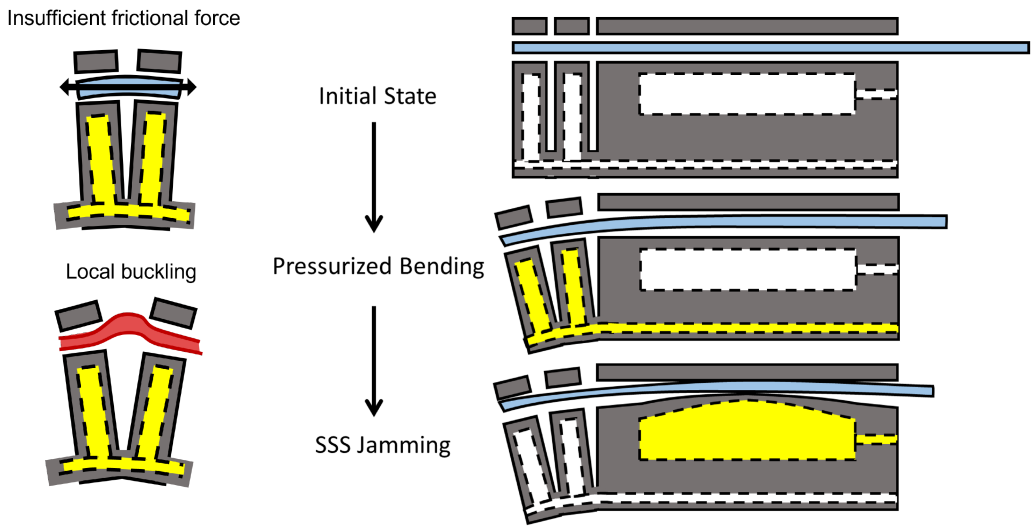

Fig. 3. Pressurizing the bending pneumatic chambers first results in pure bending of the MERA actuator. Subsequent pressurization of the jamming chamber causes the SSS to be locked in place. If the MERA encounters a payload larger than its threshold, local buckling and insufficient frictional force from the jamming chamber cause slippage of the SSS.

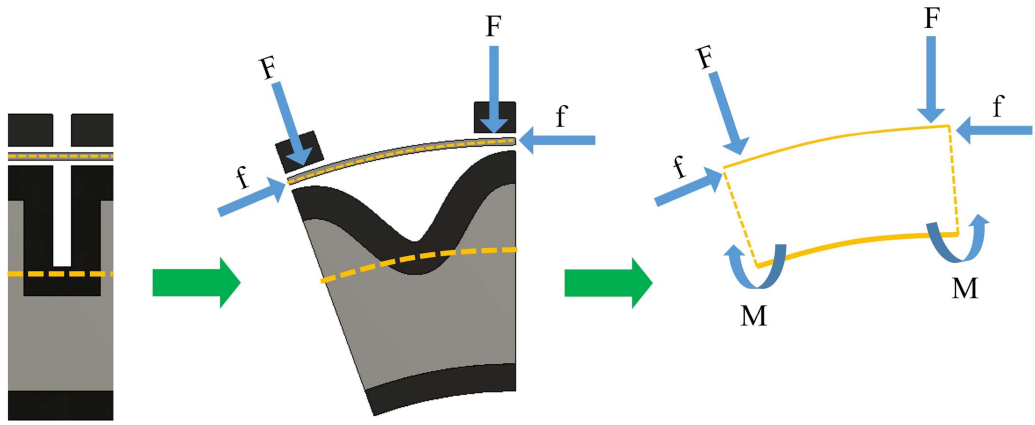

Fig. 4. Jamming unit (left) has two neutral bending axes at SSS and MERA, respectively. Distance between the axes is fixed by the normal force provided by the restraining frame. Upon actuation (middle), the SSS goes through a sliding and pure bending motion since frictional force, f, is close to 0. In a jammed state (right), sufficient frictional force is present, f, to counter the torque M created by the load and depressurization.

effective stiffness is directly proportional to the volume fraction of the constitutive materials. Consequently, larger gaps result in reduced volume fractions and lower effective stiffness. We emphasize that the present selection of gap distance is based on our prior empirical knowledge to avoid excessive manifestations of either weak or strong stiffening effects [32], [33].

The proposed jamming mechanism of MERA in our work is realized by two forces—a frictional force that prevents linear displacement of the SSS and a normal force that restrains the buckling of the SSS in each jamming unit. Input pressure to the jamming chamber can thereby determine the stiffness of the MERA. Its palmar surface is also noted to be inextensible. Consequently, the strain-limiting layer of a MERA carries out a pure bending motion upon actuation. In addition, we assume that the SSS is jammed in its pure bending state. Since the SSS possesses a high slenderness ratio, low critical buckling stress is expected. Although the SSS also has low torsional stiffness, lateral torsional buckling is neglected since the bending of the MERA is symmetric in its sagittal plane. Further studies on the effect of inserting multiple SSS were also performed and discussed in Section IV. However, it is important to note that the bending amplitude of MERA is lowered when the SSS increases in thickness and when more SSS is embedded. While the critical load is expected to increase when the thickness of SSS increases, (1) approximates the critical load when the MERA is in a bent state. We observe that MERA with increasing numbers of SSS will experience a corresponding increase in stiffness, and thus, generate different bending amplitudes at the same pressure. We report this observation in Fig. 5 and emphasize the need to evaluate the tradeoff between increasing stiffness and gripping width.

A free-body diagram of the SSS is depicted in Fig. 4 to further illustrate the jamming mechanism in the MERA. Buckling of the SSS can be deemed to be delaminated from the strain-limiting layer. This suggests that the equilibrium state of the SSS is reached by the countering forces acting locally as illustrated

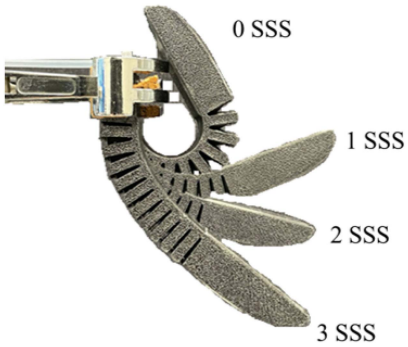

Fig. 5. Bending profile of MERA with varying numbers of SSS embedded, actuated at 140 kPa.

in Fig. 4. Similar to composite plates subjected to an in-place force compression, one with a lower modulus of elasticity tends to buckle further away from the others [42]. In our case, the buckling motion would tend to lean dorsally toward the SSS, which has a lower flexural rigidity. Given the initial prebent state of the MERA, the critical buckling load is also noted to decrease due to an eccentric load.

B. Failure Mode

Based on the assumptions above, the failure modes of the jammed finger can be categorized into two scenarios—sliding of the SSS and local flexural buckling at each jamming unit, illustrated in Fig. 3. Sliding failure occurs when the friction force between the SSS and the actuator is insufficient to prevent displacement, which could happen either at the base or the frame of the body. Since the normal force on the SSS of each jamming unit is derived from the buckling restraining frames (see Fig. 4), a larger gap between the jamming channels and a small bending angle would amplify the sliding failure between jamming units under stress; hence, in this study, the gaps are set to 1 mm to mitigate such issue. Subsequently, local buckling at a jamming unit depends on the critical load at a certain gap distance, which is correlated linearly to the bending angle of the hybrid actuator as well as the distance between the SSS and its neutral bending axis, as explained in (2). Namely, local buckling of a jamming unit tends to occur at a higher bending angle

$$L_e = L_0 + \frac{D\theta}{N} \tag{2}$$

where L_0 is the initial gap distance, N is the number of gaps, θ is the bending angle and D is the offset, given by the distance between the neutral bending axis and the SSS, which is in turn correlated to the height of the actuator. Referring to (1), the critical load of each jamming unit will decrease proportionally against the inverse of the gap distance between adjacent bellows. Therefore, local buckling can be observed more easily in thicker MERAs at smaller bending angles.

C. Fabrication

The design of the MERA was drawn in Fusion 360 (Autodesk, Inc.). Subsequently, the MERA was 3-D printed using a modified Flashforge Creator Pro printer (Flashforge, USA) equipped with a direct drive Flexion extruder (Diabase Engineering, USA). To achieve sufficient flexibility and softness of the overall finger actuator, the material adopted in this design is X60 (Diabase Engineering, USA) with a shore hardness of 60 A. The MERA was also printed with a layer height of 0.2 mm at a maximal speed of 1400 mm/min. No support structure is needed throughout this process since the pneumatic chambers are designed to be narrow (1.5 mm) to avoid overhang issues. From our experience [32], [33], the wall thickness of the pneumatic chambers should not be thinner than 1.5 mm to ensure airtightness in the actuator and improve durability. Additionally, although having more pneumatic chambers in close proximity will enhance actuator performance, we recommend that the distance between two walls be at least twice the size of the nozzle used. This minimizes the chances of unwanted adhesion due to residue build-up at the nozzle. In our work, the nozzle diameter is 0.4 mm, which in turn led to a distance of 1 mm gap between walls. The finished MERA has a smooth surface and is airtight without additional postprocessing. The SSS is 0.1 mm thick, 20 mm wide, and 150 mm in length. After the 3-D printing phase is completed, an SSS is then inserted at the proximal end of the MERA, through the restraining frames, and into the tip. The overall weight of the MERA is noted to be 82 g.

III. Modeling

Finite element (FE) simulations were conducted to investigate and validate the design concept as well as to evaluate the mechanical behavior of the actuator at different operating conditions. The X60 material used for 3-D printing the MERA was modeled using a Yeoh hyperelastic material model, with the parameters calibrated based on the stress-strain curves obtained from the tensile tests. The density of X60 was 1150 kg/m^3, and the coefficients were $C10 = 0.69$ MPa, $C20 = -7.80 \times 10^{-4}$ MPa, $C30 = 2.68 \times 10^{-6}$ MPa. Commercial FE simulation software Abaqus (Dassault System, MA) was used to model the behavior of soft actuators under external actuation. A cylinder force sensor was placed in the path of the actuator bending and was moving vertically to evaluate the reaction force of MERA under deformation. The cylinder was deemed as a rigid body in the model. The pressures applied to the main actuation chamber and jamming chamber in the FE simulations were identical to the experiments in Section IV.

The simulation was conducted in three steps. In the first step, we simulated the bending of the soft actuator with SSS inserted when the main channel was pressurized, as shown in Fig. 6(a) and (b). The distal end of the SSS was connected to the tip of the actuator, and the contact between the proximal end of the SSS and the jamming chamber of the actuator was modeled as frictional contact with a friction coefficient of 0.8. In the second step, we pressurized the jamming chamber to fix the SSS which increased the stiffness of the MERA [see Fig. 6(c)]. In the final step, we simulated the interactions between the actuator and the moving cylinder, whose speed was fixed at 13.55 $\mathrm{mm/s}$ [see Fig. 6(d) and (e)]. The dynamic analysis and explicit quasi-static analysis in Abaqus were conducted throughout the

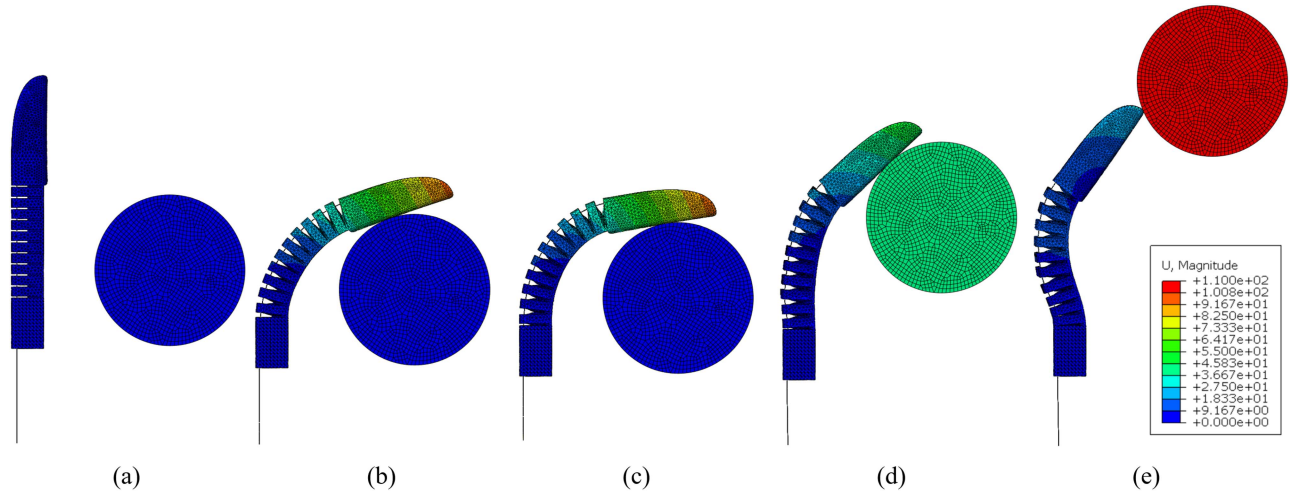

Fig. 6. Finite element simulation results of the actuation process and the interactions between the actuator and the moving cylinder. (a) Initial state of the actuator with a SSS inserted. (b) Final state of the actuator after applying pressure in the main channel. (c) Final state of the actuator after applying pressure in the jamming channel. (d) Intermediate state of the actuator while the cylinder is moving upwards. (e) Final state of the actuator when the cylinder is leaving the contact region.

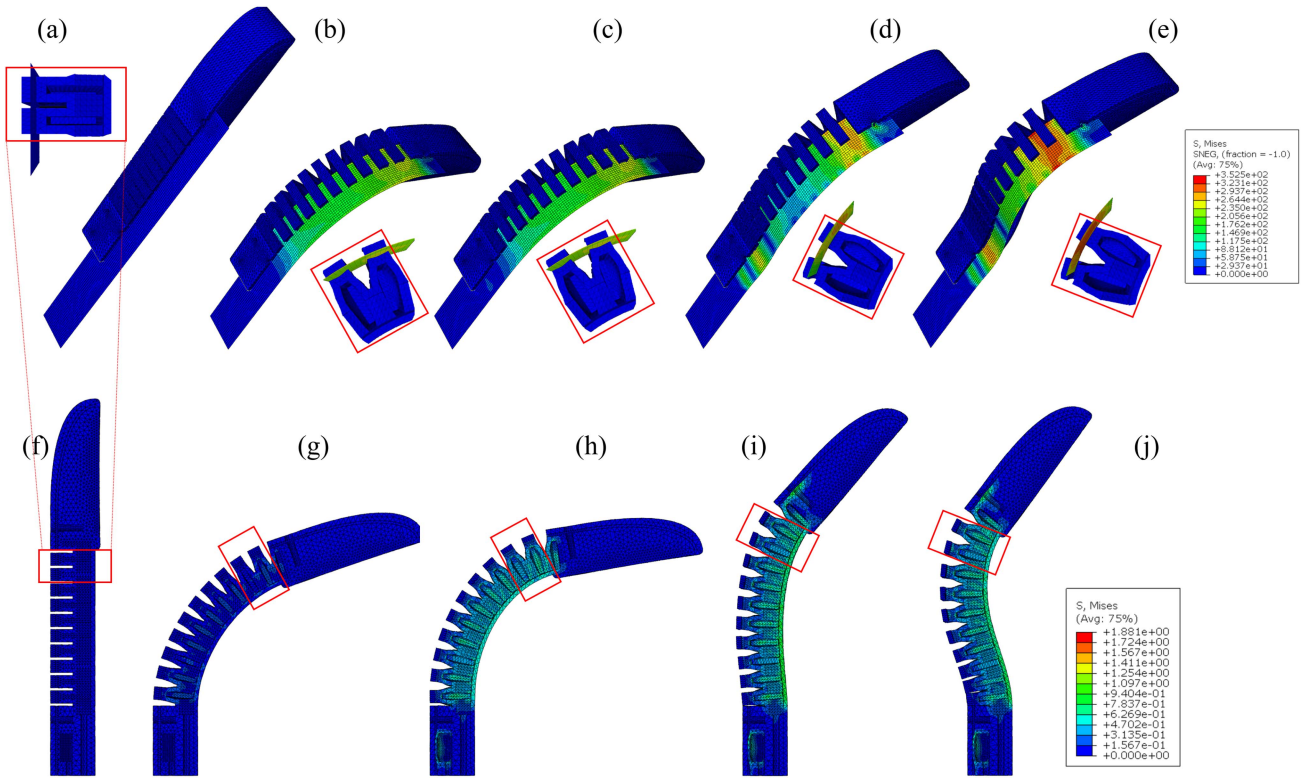

Fig. 7. FE simulation results of the stress distribution within the actuator and the SSS. (a)–(e) give the Mises stress evolution for both the finger and SSS, showing that SSS is bearing most of the stress induced by the system. (f)–(j) Mises stress distribution within the finger only, indicating that the stress level within the finger is much lower than that in the SSS. The insets in (a)–(e) are enlarged views of two units within the red boxes shown in (f)–(j). (a)–(f) Initial state. (b)–(g) Final state of the actuator after applying pressure in the main channel. (c)–(h) Final state of the actuator after applying pressure in the jamming channel. (d)–(i) Middle state of the actuator when the cylinder is moving upwards. (e) and (j) Final state of the actuator when the cylinder is leaving the contact region.

three steps with a default automatic time increment no greater than 0.1 s. The calculation time was 1 s for the first two steps and 10 s for the final step. The frictional contact between the actuator and the cylinder was modeled with a friction coefficient of 0.7.

In response to the displacement, the stress distribution of the MERA throughout the entire process is illustrated in Fig. 7 and presented in Movie S1. Since the stress concentration of the SSS is located at the base and the distal end of the fingertip, we presume the failure of fatigue or buckling to happen during

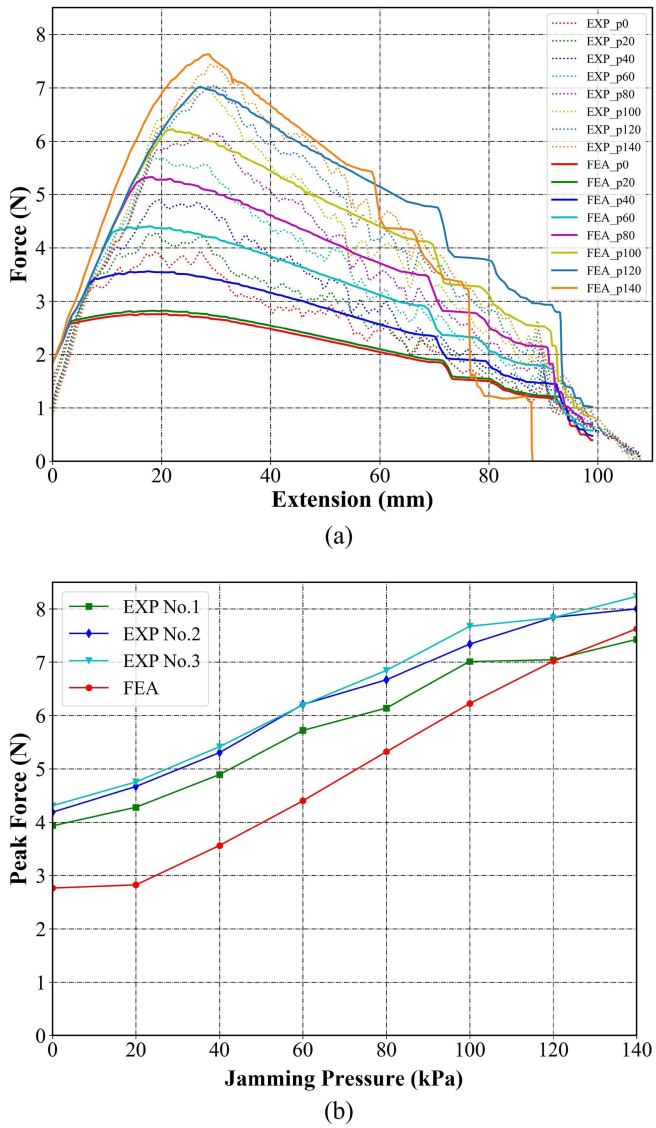

Fig. 8. (a) FEA simulation results versus experimental results (experiment No. 1). (b) Simulated peak contact force at different applied pressures in the jamming channel.

fatigue tests in similar areas, further validation is conducted in Section IV.

Fig. 8(a) plots the simulated and measured contact forces in the final step against the moving displacement of the cylinder with different jamming pressures, which was applied in step 2. In both FE simulations and experiments, the contact force first increases linearly to a peak value. It then gradually decreases to zero when the cylinder moves up and eventually leaves the contact region. The initial slope of the contact forces in the simulation agrees well with the experimental results. During this phase, the mechanical behavior of the actuator is dominated by the inserted SSS, while the pressure applied in the jamming channel has limited influence. In the later phases, the stiffening effect induced by the jamming pressure starts to take over, resulting in higher peak forces at higher jamming pressures. Fig. 8(b) illustrates the simulated and measured peak forces at different jamming pressures.

Essentially, FE simulation can capture the trends that the peak force is approximated to be increasing linearly with the jamming pressure. According to (1), the critical load is proportional to the effective stiffness of the finger. When only the jamming pressure is changing, the variation of the peak force is equivalent to the variation of the stiffness. Therefore, from Fig. 8(b), we can see that both the experiments and simulation demonstrate that the overall stiffness of the finger, namely the effective stiffness in (1), is almost increasing linearly with the jamming pressure. However, slight discrepancies are also evident in terms of the magnitudes of the peak force, especially when the jamming pressure applied is low. Additionally, the simulated contact forces in the later stage are higher compared to the experiments and exhibit "staircase-shaped" behaviors during the final phase of the contact interaction. Several reasons may account for the discrepancies and mismatch. First, the material parameters used in the simulation are evaluated with the as-print dog-bone tensile specimen. However, given the inherent hyperelastic material properties of the MERA, the printed actuator may not exhibit the exact material parameters and its material properties may also change over time. This uncertainty causes errors in accurately modeling the reaction force, especially in a complex stress state and highly nonlinear mechanical behavior. Second, the actual slipping phenomenon between the SSS and the actuator, or between the actuator and the cylinder are challenging conditions that may not be fully captured in the simulations. In the current FE model, we assume the entire process to be quasi-static, and the frictional forces are computed with estimated constant static friction coefficients. However, in the later contact phases, the cylinder is sliding across the tip of the actuator, and the process may have experienced a lower friction coefficient, which could lead to lower reaction forces. The staircase-shaped curves from the simulation are possibly caused by numerical instabilities that occur only when the tip edge of the actuator is in contact with the cylinder.

Despite these uncertainties and challenges in the FE model, the simulation still captures key phenomena and trends in the experiment. This enables us to better understand the reinforcement effect of the inserted SSS, as well as the degree to which jamming pressure may influence the stiffness of an actuated MERA. Furthermore, with the aid of the current model, the force output of the MERA can be optimized based on the desired stiffness and reaction force.

IV. Actuator Characterization

A. Experimental Setup

1) Tip Force Characterization: In this section, we first investigate the effect of inserting different quantities of SSS and the magnitude of tip force acting on cylinders of different diameters. With both bending and jamming pressure arbitrarily set to 140 kPa, the effect of inserting multiple SSS is reported in Figs. 5 and 9. Although the experimental setup is fixed (see Fig. 9), the point of contact between MERA and the cylindrical block is observed to differ slightly depending on the input parameters (see Table I). Hence, we investigate the relationship between the tip force applied by the MERA and the size of the cylindrical

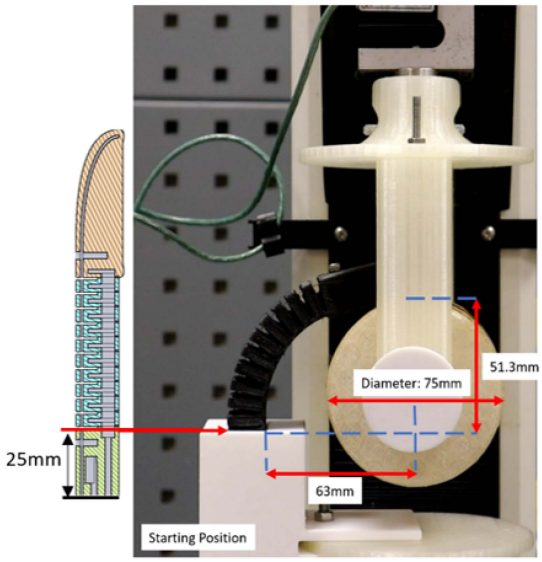

Fig. 9. Experimental setup used to measure tip force exerted by the MERA. A cylinder is placed in the path of the MERA during bending. Subsequent upward motion generates an equal reaction force that is recorded throughout the entire process.

TABLE I
INPUT PARAMETERS OF THE EXPERIMENT SETUP

Bending pressure	140 kPa
Jamming pressure	0—140 kPa
Cylinder size	25/50/75 mm in diameter
No. of SSS	1—3

object. An experimental setup (see Fig. 9) is used to characterize the MERA and the input parameters of each iteration are as summarized in Table I. Jamming pressure, cylinder size, and number of SSS inserted into the finger are variables while the distance at which the MERA and its orientation with respect to the radial axis of the cylinder are constant. The center axes of the cylinders are positioned at the base of the actuator consistently and pulled upwards until the actuator slips out of the rig, as simulated in Fig. 6. Additionally, jamming pressure is set with an arbitrary range of 0–140 kPa with a 20 kPa increment per iteration. With reference to Movie S2, the function of jamming can be seen as creating a temporarily inextensible layer of SSS throughout the restraining frame, which leads to an extension motion when the actuation sequence is reversed. Hence, as shown in Fig. 3, the actuation sequence is predetermined to be bending-first for all the following tests in this study. The identical actuation sequence is adopted in the FE simulations described in Section III.

2) MERA-Gripper Holding Force: A rig in Fig. 10 was built to investigate the holding force of the MERA-Gripper. The diameter of the cylinder is 75 mm and the gripping width is fixed at 90 mm. The MERA-gripper consists of three MERAs in this experiment. The holding force of the gripper is recorded throughout the three repetitions with and without the SSS installed.

3) Fatigue Test: The actuator is susceptible to fatigue and failure after extended periods of use. Cyclical expansion and contraction of the pneumatic chambers will inevitably cause the walls to degrade over time. To quantify the fatigue endurance of MERA, 0–140 kPa of cyclical pressurization is applied. The actuator is considered fatigued when it is unable to sustain the upper limit of 140 kPa internally due to the walls rupturing.

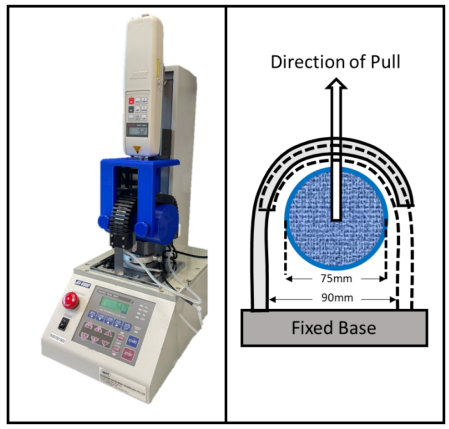

Fig. 10. Experimental setup (left) and schematic diagram (right) for testing MERA-Gripper holding force. The upward motion of the cylinder generates a reaction force equal to the gripping force that is recorded throughout the process.

B. Results

1) Tip Force Characterization: The MERA was first tested without the SSS reinforcement and yielded a peak force of 2 N as shown in Fig. 11(a). Modulation of stiffness is done using varying jamming pressure from 0 to 140 kPa. Results show that the higher the jamming pressure, the better the force readings. Thus, an operational jamming pressure and upper limit of 140 kPa were eventually decided upon and used for subsequent experiments. On the other hand, force readings obtained are studied with the actuation pressure stabilizing at 140 kPa. Notably, during the third trial of the MERA with one SSS, a lower force profile was measured resulting in a larger standard deviation [see Fig. 11(b)], owing to the occurrence of local buckling between bellows. Despite the observed buckling failure, the MERA with one SSS inserted still managed to gain a 291% increase in the maximum tip force compared to the MERA without any SSS inserted.

As discussed in Section II-B, the determination of the tip force is highly related to two factors, the critical load of each jamming unit and the frictional force at the jamming chamber. Respectively, it would lead to the local buckling between chambers and the sliding of the SSS at failure. From Fig. 11(b)–(d), we could see a clear improvement of tip force with the second SSS installed [see Fig. 11(c)], where both of the SSS have one side in contact with the jamming chamber directly, which possesses a higher frictional coefficient. With the third SSS installed, the middle SSS sandwiched in between would get a much lower frictional coefficient, which leads to sliding failure easily. Hence, embedding three and above of the SSS would not necessarily improve on the maximum tip force exponentially, due to the delamination of SSS and the reduction in friction force.

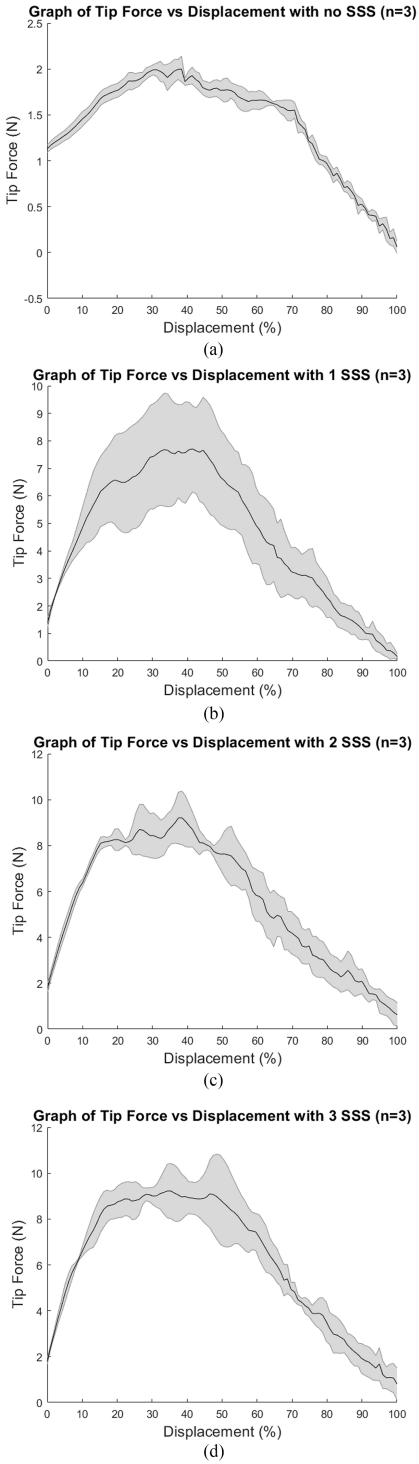

Fig. 11. Tip force with respect to cylinder displacement at 140 kPa jamming pressure using the large cylinder (75 mm in diameter) with (a) 0 SSS, (b) 1 SSS, (c) 2 SSS, and (d) 3 SSS installed in the MERA, respectively. Three repetitions (n=3) are conducted per experimental run.

Tip force recorded from cylinders of three different sizes is presented in Fig. 12. We note that cylinders with larger diameters result in a smaller degree of bending in the MERA and shift the contact point closer with respect to the base of the MERA. Hence, an increase in tip force is observed. Referencing (1) and (2), the increase in L_e by bending of the MERA leads to a smaller critical load between the bellows, resulting in local flexural buckling. Furthermore, when the contact point is closer to the base of the MERA, a smaller countering torque would be required to maintain equilibrium. Therefore, we can conclude that the MERA is able to grasp larger objects more firmly than smaller ones with the same mass.

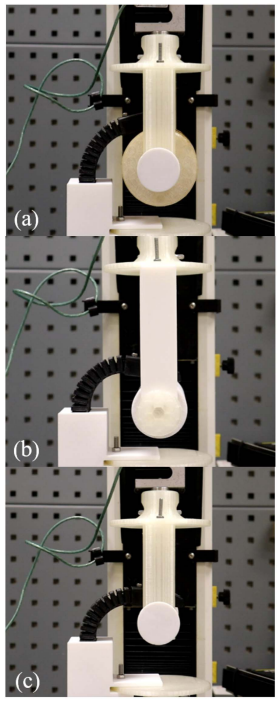

Peak force (N)	0 metal strap	1 metal strap	2 metal strip	3 metal strip
Small Block	1.6601 ± 0.0611	3.9930 ± 0.1300	5.3517 ± 0.4962	6.0091 ± 0.9222
Medium Block	3.5810 ± 0.2367	6.1629 ± 0.8944	6.3988 ± 1.5497	7.0730 ± 1.7613
Large Block	2.0439 ± 0.1019	7.9999 ± 1.8206	9.5458 ± 0.6514	9.7688 ± 0.7486

Fig. 12. Tip force test with three different diameters of cylinders. (a) Small (25 mm). (b) Medium (50 mm). (c) Large (75 mm). The shown table is the average and standard deviation of the peak force among three trials alternately, where the jamming pressure of 140 kPa is applied.

2) MERA-Gripper Holding Force: As shown in Fig. 13, the holding force of the gripper yielded a peak force of 23.5 N without the reinforcement of SSS. The data are with low variation, which indicates the repeatability of the actuator. With the embedded SSS jamming at 140 kPa, the holding force onto the rig reaches 41.5 N on average among the three repetitions. The MERA-gripper gains an average of 76.5% growth in maximum holding force with respect to the gripper in the absence of the SSS. Nonetheless, given the frictional and planar buckling factors for embedded SSS in each repetition, the variation of the holding force beyond the maximum is larger, respectively. A slower extension rate caused by the frictional force between the frame and the SSS is also noticed at 100% displacement, as shown in Movie S3.

3) Fatigue Test: Subjecting three MERAs to 0–140 kPa cyclical pressurization, an average of 79 973 ± 6978 cycles

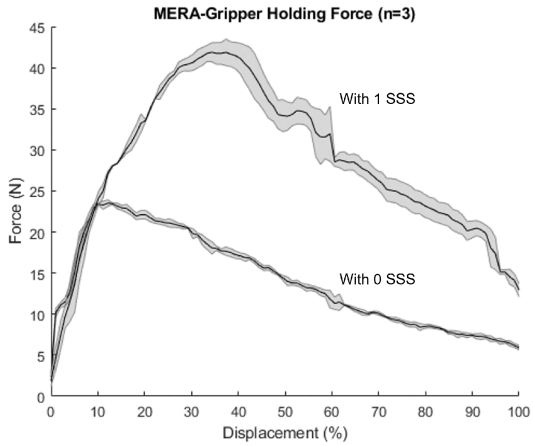

Fig. 13. Holding force of the MERA-Gripper measured by the experimental setup in Fig. 10. Three repetitions (n=3) are conducted per experimental run. Apparent advantages in payload and gripping stability were observed from the profile of the MERA with the jamming function on.

Item	Weight
Powder package	415g
Powder bottle	500g
Sugar package	1000g
Soft drink bottle	1600g
Power drill	1600g
Dumbbell	2000g
Oil bottle	3400g

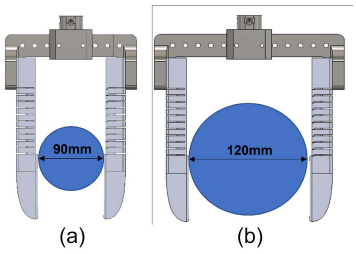

Fig. 14. On the left, items of the pick-and-place demonstration and their corresponding weight are listed. On the right, the two fixed gripping widths (a) & (b) of the MERA-gripper adopted in Fig. 15 are illustrated.

is recorded before air leakage is observed. It is noteworthy that air leakage occurred due to small tears between the folds of the actuator nearer its distal end. This observation corresponds to our simulation where larger stresses and strains are to be expected at these regions (see Fig. 7), thereby contributing to the relatively faster rate of rupturing.

V. Applications

In this section, a gripper adopting three MERAs is mounted on a robotic arm to demonstrate its grasp stability and payload capabilities (see Fig. 14). As shown in Fig. 15, the gripper is put through a simple holding test with various products of different sizes and weights, with two different gripping width configurations. Ranging from 415 g to 3.4 kg, the short-listed items come in the shape of cylindrical handles or pouches and have different contact surfaces with the gripper. The input pressure for both the actuation and jamming chamber is set to be 140 kPa throughout the test. The success of SSS-reinforced gripping is demonstrated in Movie S3. For the first few items with a lighter weight (415 g–1 kg), the MERA-gripper was able to hold them firmly regardless of the gripping width and item shapes. Although the contact surfaces of the packages are deformable and contact points are distributed over the palmar surface of the MERA-gripper, better grasp stability and higher success rates of gripping are observed. Subsequently, the MERA-gripper failed to pick up the soft drink bottle, weighing 1.6 kg, without the reinforcement of the jamming function at both gripping widths. As observed in Movie S4, the liquid within the bottle leads to a fluctuating centre of gravity during the impact and transport of the bottle. This phenomenon is amplified during manipulation and fast movements of the items, which in turn causes the increase of stress in the base of the gripper and results in gripping instability. On the other hand, the same issue is vastly mitigated when the jamming function is ON, corresponding to our aforementioned findings in Section IV-B Nonetheless, the gripping base of the MERA still needs to withstand a higher torque when the high payload is further away from the base of the MERA or imbalanced between different actuators. The power drill with a heavier end is creating a stress load imbalance within the gripper. At a smaller gripping width, the magnitude of this stress load is reduced due to the decrease in torque required from the MERA. On the other hand, despite the heavier weight, a well-balanced dumbbell could be easily picked up at the same gripping width.

As mentioned above in Section IV-B, bigger-sized objects within a configured gripping width could also aid in increasing the payload. The result in Fig. 15 epitomizes this observation in our tip force test with varying sizes of cylinders. Subsequently, a demonstration of load bearing by simply relying on the effect of buckling restraining is also presented in Movie S3.

VI. Discussion

Fabrication of complex shaped soft grippers remains a challenge because modern day soft actuators possess impractical geometries to attain desired bending profiles and load-bearing capabilities. If not manually molded, Bell et al. [44] showed that requirements for automated injection molding of soft actuators are rigid. Machining of durable metal molds is limited to simple bellow designs. Soft actuators with multiple cavities will then face many difficulties and lower success rates. Although 3-D printed molds and soft cores can be used to circumvent design limitations, durability becomes a concern as surface finishing and poor resolution introduce cracks into the walls. Moreover, should inhomogeneous materials need to be embedded, manual intervention is still needed. Therefore, there is much benefit toward directly 3-D printing a soft actuator with more than one cavity or material. We demonstrate that a normally tedious and multiphasic fabrication process can be automated and simplified through direct 3-D printing without sacrificing durability and performance.

In addition, with our novel SSS reinforcement, the three-fingered MERA gripper has demonstrated its ability to exert average peak vertical pulling forces of 41.5 ± 1.2 N (see Fig. 13), which yields to an average of 13.8 N per actuator. An average peak vertical grip force of 8.0 ± 1.8 N [see Fig. 11(b)] is also recorded per finger actuator. A comparison table of holding force between the MERA-gripper and prior studies is also presented in Table II. The advantage of layer jamming via positive pressure is evidently presented in the peak holding force output at its

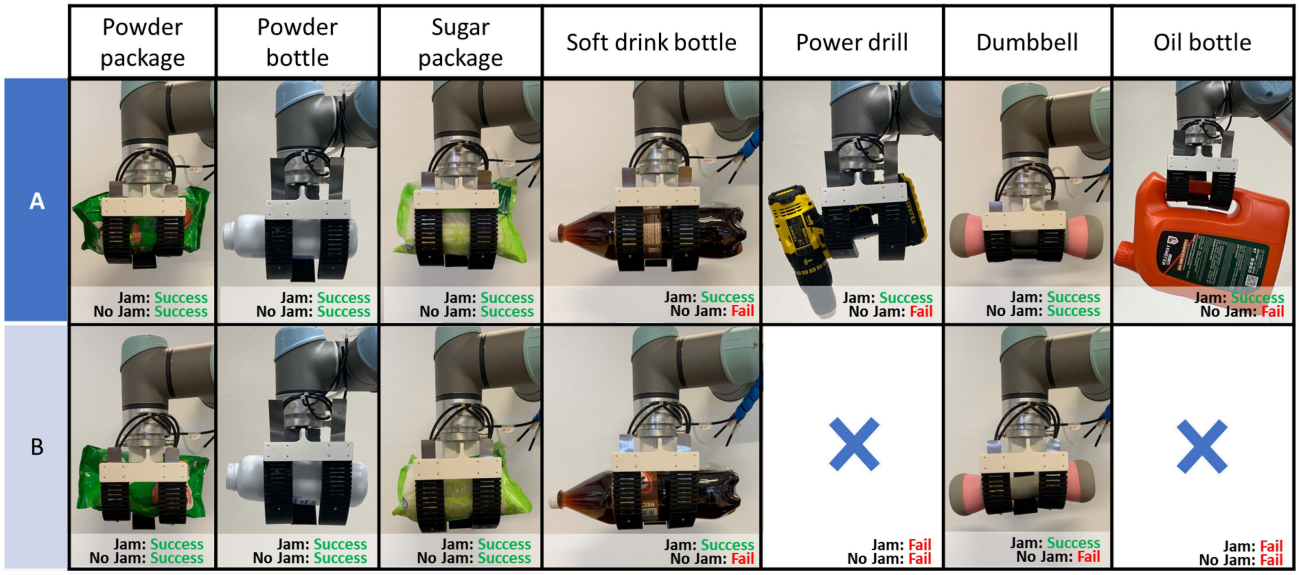

Fig. 15. Demonstration of grasp stability of a gripper equipped with three MERA-design fingers. The base can be reconfigured to two different widths and subsequently mounted onto a robotic arm which is programmed to pick items of different sizes and weights. Each item is gripped by the MERA-gripper in two different gripping widths (see Fig. 14) both with and without the jamming function accordingly.

TABLE II
GRIPPING PEAK FORCE OUTPUT COMPARISON WITH PREVIOUS STUDIES OF JAMMING REINFORCED ACTUATOR

Source	Variable stiffness tuning method	Peak holding force output (per actuator)
Passive particle jamming soft actuator [24]	Passive particle jamming upon actuation	approximately 5.58N
Variable stiffness soft actuator [25]	Granular jamming via vacuum	approximately 7N
Variable stiffness structure (VSS) [26]	Thermally activated phase change material	8.1N
Variable stiffness particle phalange (VSPP) [27]	Passive particle jamming upon contact	9.7N
3D printed rotational layer jamming unit (RLJ) [45]	Layer jamming via vacuum	3.6N
Palm-shape variable-stiffness gripper [46]	Fabric jamming via vacuum	8.5N
3D printed positive pressure jamming gripper [47]	Layer jamming via positive pressure	40N
3D printed MERA gripper	Layer jamming via positive pressure	13.8N

jammed state. Nonetheless, despite the lower peak holding force output due to the profile of the actuating unit, the slender profile of the MERA gripper makes it more suitable for insertion into cluttered and narrow spaces. Moreover, unlike other metal-infused grippers, our work features a near-instantaneous actuation, which is paramount for fast pick-and-place applications. However, the durability of MERA leaves much to be desired. Given that MERA lasts an average of 79 973 cycles before observable leakage, much improvement, and design optimization is needed to reach numbers in the millions. Nonetheless, in its current form, the MERA gripper can be reconfigured to grasp items of various sizes and has shown to be capable of picking a wide variety of commercial products.

VII. CONCLUSION

In summary, we presented our work on a MERA that used a SSS to modulate its stiffness. We also described its design rationale and elaborated on the fabrication steps needed to ensure successful 3-D printing of said actuator. A finite element model was built and simulation was done to predict the force output of the MERA. We also studied the effects of inserting multiple SSSs on measured tip force. A 291% increase in maximal tip force was observed in the SSS-reinforced MERA compared to one without. It is noteworthy that inserting multiple SSSs did not impact maximal tip force significantly. Finally, we adapted the MERA into a reconfigurable gripper end effector and demonstrated that SSS reinforcement was indeed needed to enhance the grasp stability of certain objects that possess challenging physical properties.

Variable stiffness was an important characteristic that was necessary for soft actuators to improve their payload before they could be deployed in industrial settings with highly varied grasping requirements. While the concept of reinforcing soft actuators with metallic structures was not novel, our methodology provided an automated and repetitive way in which they could be fabricated through 3-D printing. Unlike contemporary variable stiffness soft actuators made through manual means, the 3-D printed MERAs here were identical and had similar performance to one another. 3-D printing hence allowed scalability and reduced dependence on an individual's mastery.

Additionally, the SSS jamming mechanism was simple to operate, and incorporation into an existing bending actuator could be done easily. Given the multitude of actuator designs, SSS reinforcement can be widely applied to improve the payload

of soft actuators. More significantly, the SSS was also thin and lightweight. Therefore, such an augmentation will not alter the original profile radically.

In future, several steps can be taken to improve the force and stiffness tuning performance. Any increment in absolute force would entail fabricating the actuator with a different material that is softer than 60 A shore hardness. The actuator's design can be adjusted, such as through segmentation into multiple finger joints or modification of the size of pneumatic chambers, in order to optimize the force output. The investigation of flexural rigidity in splints made from various materials is also essential for achieving improved robustness.

In conclusion, we believe that our work is paramount toward the large-scale adoption of soft robotic grippers in industrial automation applications. Through the MERA presented here, we believe that major obstacles in grasp stability and payload can be overcome toward pick-and-place applications using soft robotic grippers.

References

[1] C. Melchiorri and M. Kaneko, *Robot Hands*. Berlin, Germany: Springer, 2016, pp. 463–480.

[2] B. K. O. Siciliano, "Springer handbook of robotics," 2008. [Online]. Available: https://link.springer.com/book/10.1007/978-3-540-30301-5

[3] J. Krüger et al., "Innovative control of assembly systems and lines," *CIRP Ann.*, vol. 66, no. 2, pp. 707–730, 2017. [Online]. Available: https://www.sciencedirect.com/science/article/pii/S000785061730149X

[4] G. Michalos, S. Makris, N. Papakostas, D. Mourtzis, and G. Chryssolouris, "Automotive assembly technologies review: Challenges and outlook for a flexible and adaptive approach," *CIRP J. Manuf. Sci. Technol.*, vol. 2, no. 2, pp. 81–91, 2010. [Online]. Available: https://www.sciencedirect.com/science/article/pii/S1755581709000467

[5] R. Pfeifer, M. Lungarella, and F. Iida, "The challenges ahead for bio-inspired 'soft' robotics," *Commun. ACM*, vol. 55, no. 11, pp. 76–87, 2012, doi: 10.1145/2366316.2366335.

[6] L. Wang and F. Iida, "Deformation in soft-matter robotics: A categorization and quantitative characterization," *IEEE Robot. Autom. Mag.*, vol. 22, no. 3, pp. 125–139, Sep. 2015.

[7] C. Linghu et al., "Universal SMP gripper with massive and selective capabilities for multiscaled, arbitrarily shaped objects," *Sci. Adv.*, vol. 6, no. 7, 2020, Art. no. eaay5120, doi: 10.1126/sciadv.aay5120.

[8] J. Shintake, V. Cacucciolo, D. Floreano, and H. Shea, "Soft robotic grippers," *Adv. Mater.*, vol. 30, no. 29, 2018, Art. no. 1707035, doi: 10.1002/adma.201707035.

[9] J. Hughes, U. Culha, F. Giardina, F. Guenther, A. Rosendo, and F. Iida, "Soft manipulators and grippers: A review," *Front. Robot. AI*, vol. 3, pp. 2–3, 2016. [Online]. Available: https://www.frontiersin.org/articles/10.3389/frobt.2016.00069

[10] L. Zhou, L. Ren, Y. Chen, S. Niu, Z. Han, and L. Ren, "Bio-inspired soft grippers based on impactive gripping," *Adv. Sci.*, vol. 8, no. 9, 2021, Art. no. 2002017, doi: 10.1002/advs.202002017.

[11] S. Song, C. Majidi, and M. Sitti, "GeckoGripper: A soft, inflatable robotic gripper using gecko-inspired elastomer micro-fiber adhesives," in *Proc. IEEE/RSJ Int. Conf. Intell. Robot. Syst., Conf. Proc.*, 2014, pp. 4624–4629.

[12] J. Amend, N. Cheng, S. Fakhouri, and B. Culley, "Soft robotics commercialization: Jamming grippers from research to product," *Soft Robot.*, vol. 3, no. 4, pp. 213–222, 2016, doi: 10.1089/soro.2016.0021.

[13] E. Brown et al., "Universal robotic gripper based on the jamming of granular material," *Proc. Nat. Acad. Sci.*, vol. 107, no. 44, pp. 18809–18814, 2010, doi: 10.1073/pnas.1003250107.

[14] T. Zhu, H. Yang, and W. Zhang, "A spherical self-adaptive gripper with shrinking of an elastic membrane," in *Proc. Int. Conf. Adv. Robot. Mechatronics*, 2016, pp. 512–517.

[15] J. R. Amend, E. Brown, N. Rodenberg, H. M. Jaeger, and H. Lipson, "A positive pressure universal gripper based on the jamming of granular material," *IEEE Trans. Robot.*, vol. 28, no. 2, pp. 341–350, Apr. 2012.

[16] S. Li et al., "A vacuum-driven origami "magic-ball" soft gripper," in *Proc. Int. Conf. Robot. Autom.*, 2019, pp. 7401–7408. .

[17] Y. Hao et al., "A multimodal, enveloping soft gripper: Shape conformation, bioinspired adhesion, and expansion-driven suction," *IEEE Trans. Robot.*, vol. 37, no. 2, pp. 350–362, Apr. 2021.

[18] S. Zaidi, M. Maselli, C. Laschi, and M. Cianchetti, "Actuation technologies for soft robot grippers and manipulators: A review," *Curr. Robot. Rep.*, vol. 2, no. 3, pp. 355–369, 2021, doi: 10.1007/s43154-021-00054-5.

[19] J. Meng, L. Gerez, J. Chapman, and M. Liarokapis, "A tendon-driven, preloaded, pneumatically actuated, soft robotic gripper with a telescopic palm," in *Proc. IEEE 3rd Int. Conf. Soft Robot.*, 2020, pp. 476–481.

[20] I. De Falco, M. Cianchetti, and A. Menciassi, "A soft multi-module manipulator with variable stiffness for minimally invasive surgery," *Bioinspiration Biomimetics*, vol. 12, 2017, Art. no. 056008.

[21] K. Lee, Y. Wang, and C. Zheng, "TWISTER hand: Underactuated robotic gripper inspired by origami twisted tower," *IEEE Trans. Robot.*, vol. 36, no. 2, pp. 488–500, Apr. 2020.

[22] C. Tawk, Y. Gao, R. Mutlu, and G. Alici, "Fully 3D printed monolithic soft gripper with high conformal grasping capability," in *Proc. IEEE/ASME Int. Conf. Adv. Intell. Mechatron.*, 2019, pp. 1139–1144.

[23] D. Venter and S. Dirven, "Self morphing soft-robotic gripper for handling and manipulation of delicate produce in horticultural applications," in *Proc. 24th Int. Conf. Mechatron. Mach. Vis. Pract.*, 2017, pp. 1–6.

[24] Y. Li, Y. Chen, Y. Yang, and Y. Wei, "Passive particle jamming and its stiffening of soft robotic grippers," *IEEE Trans. Robot.*, vol. 33, no. 2, pp. 446–455, Apr. 2017.

[25] J. Hu, L. Liang, and B. Zeng, "Design, modeling, and testing of a soft actuator with variable stiffness using granular jamming," *Robotica*, vol. 40, no. 7, pp. 2468–2484, 2022, doi: 10.1017/S0263574721001740.

[26] T. T. Hoang, P. T. Phan, M. T. Thai, N. H. Lovell, and T. N. Do, "Bio-inspired conformable and helical soft fabric gripper with variable stiffness and touch sensing," *Adv. Mater. Technol.*, vol. 5, no. 12, 2020, Art. no. 2000724, doi: 10.1002/admt.202000724.

[27] J. Zhou et al., "Adaptive variable stiffness particle phalange for robust and durable robotic grasping," *Soft Robot.*, vol. 7, no. 6, pp. 743–757, 2020, doi: 10.1089/soro.2019.0089.

[28] M. Henke and G. Gerlach, "On a high-potential variable-stiffness device," *Microsystem Technol.*, vol. 20, no. 4, pp. 599–606, 2014, doi: 10.1007/s00542-013-1995-5.

[29] H. Yufei et al., "A variable stiffness soft robotic gripper with low-melting-point alloy," in *Proc. 36th Chin. Control Conf.*, 2017, pp. 6781–6786.

[30] R. Deimel and O. Brock, "A novel type of compliant and underactuated robotic hand for dexterous grasping," *Int. J. Robot. Res.*, vol. 35, pp. 2–4, 2015, doi: 10.1177/0278364915592961.

[31] J. Zhou, S. Chen, and Z. Wang, "A soft-robotic gripper with enhanced object adaptation and grasping reliability," *IEEE Robot. Autom. Lett.*, vol. 2, no. 4, pp. 2287–2293, Oct. 2017.

[32] B. A. W. Keong and R. Y. C. Hua, "A novel fold-based design approach toward printable soft robotics using flexible 3D printing materials," *Adv. Mater. Technol.*, vol. 3, no. 2, 2018, Art. no. 1700172. [Online]. Available: https://doi.org/10.1002/admt.201700172 https://onlinelibrary.wiley.com/doi/abs/10.1002/admt.201700172

[33] C. Y. Chen, K. P. May, and C. H. Yeow, "3D printed soft extension actuator," in *Proc. IEEE 4th Int. Conf. Soft Robot.*, 2021, pp. 435–441.

[34] C. Tawk, M. in het Panhuis, G. M. Spinks, and G. Alici, "Bioinspired 3D printable soft vacuum actuators for locomotion robots, grippers and artificial muscles," *Soft Robot.*, vol. 5, no. 6, pp. 685–694, 2018, doi: 10.1089/soro.2018.0021.

[35] D. K. Patel, A. H. Sakhaei, M. Layani, B. Zhang, Q. Ge, and S. Magdassi, "Highly stretchable and uv curable elastomers for digital light processing based 3D printing," *Adv. Mater.*, vol. 29, no. 15, 2017, Art. no. 1606000, doi: 10.1002/adma.201606000.

[36] T. Hainsworth, L. Smith, S. Alexander, and R. MacCurdy, "A fabrication free, 3D printed, multi-material, self-sensing soft actuator," *IEEE Robot. Autom. Lett.*, vol. 5, no. 3, pp. 4118–4125, Jul. 2020.

[37] R. L. Truby et al., "Soft somatosensitive actuators via embedded 3 D printing," *Adv. Mater.*, vol. 30, no. 15, 2018, Art. no. 1706383, doi: 10.1002/adma.201706383.

[38] Y.-F. Zhang et al., "Fast-response, stiffness-tunable soft actuator by hybrid multimaterial 3D printing," *Adv. Funct. Mater.*, vol. 29, no. 15, 2019, Art. no. 1806698, doi: 10.1002/adfm.201806698.

[39] X.-Y. Guo, W.-B. Li, Q.-H. Gao, H. Yan, Y.-Q. Fei, and W.-M. Zhang, "Self-locking mechanism for variable stiffness rigid–soft gripper,"," *Smart Mater. Structures*, vol. 29, no. 3, 2020, Art. no. 035033, doi: 10.1088/1361-665X/ab710f.

[40] G. Domokos, P. Holmes, and B. Royce, "Constrained euler buckling," *J. Nonlinear Sci.*, vol. 7, pp. 281–314, 1997.
[41] H. Chai, "Contact buckling and postbuckling of thin rectangular plates," *J. Mechanics Phys. Solids*, vol. 49, no. 2, pp. 209–230, 2001. [Online]. Available: https://www.sciencedirect.com/science/article/pii/S0022509600000387
[42] A. D. Muradova and G. E. Stavroulakis, "Mathematical models with buckling and contact phenomena for elastic plates: A review," *Mathematics*, vol. 8, no. 4, 2020, Art. no. 566.
[43] Z. Hashin and S. Shtrikman, "A variational approach to the theory of the elastic behaviour of multiphase materials," *J. Mechanics Phys. Solids*, vol. 11, no. 2, pp. 127–140, 1963. [Online]. Available: https://www.sciencedirect.com/science/article/pii/0022509663900607
[44] M. A. Bell, K. P. Becker, and R. J. Wood, "Injection molding of soft robots," *Adv. Mater. Technol.*, vol. 7, no. 1, 2022, Art. no. 2100605, doi: 10.1002/admt.202100605.
[45] M. Zhu, M. Xie, Y. Mori, J. Dai, S. Kawamura, and X. Yue, "A variable stiffness soft gripper based on rotational layer jamming," *Soft Robot.*, vol. 11, pp. 85–94, 2023, doi: 10.1089/soro.2022.0232.
[46] Y. Zhao and Y. Wang, "A palm-shape variable-stiffness gripper based on 3D-printed fabric jamming," *IEEE Robot. Autom. Lett.*, vol. 8, no. 6, pp. 3238–3245, Jun. 2023.
[47] G. B. Crowley, X. Zeng, and H.-J. Su, "A 3D printed soft robotic gripper with a variable stiffness enabled by a novel positive pressure layer jamming technology," *IEEE Robot. Autom. Lett.*, vol. 7, no. 2, pp. 5477–5482, Apr. 2022, doi: 10.1109/LRA.2022.3157448.

Chao-Yu Chen received the bachelor's degree in mechanical engineering from National Taiwan University, Taipei, Taiwan, in 2018, and the master's degree in biomedical engineering from the National University of Singapore, Singapore, in 2022.

He is currently a Research Associate with Evolution Innovation Lab, National University of Singapore, headed by Associate Professor Raye Yeow Chen Hua. He is also a cofounder of a soft robotics startup founded in 2021.

Benjamin Wee Keong Ang received the Ph.D. degree in biomedical engineering from the National University of Singapore, Singapore, in 2022.

He is currently a Research Fellow under the NUS Resilience & Growth Postdoctoral Fellowship Programme with Evolution Innovation Lab, headed by Associate Professor Raye Yeow Chen Hua. His research interests include the design and fabrication of soft robots, soft wearables, and industrial automation using soft end effectors.

Yangfan Li Yangfan Li received the Ph.D. degree in structural engineering from Swinburne University of Technology, Melbourne, Australia, in 2018.

She is currently a Research Scientist with the Institute of High-Performance Computing, Agency for Science, Technology and Research, Singapore. Her main research interests include topology optimization of multifunctional structures, multiscale modeling and optimization of artificial metamaterials and composites, and soft, and continuum robotics modeling.

Jun Liu (Member, IEEE) received the Ph.D. degree in mechanical engineering from National University of Singapore (NUS), Singapore, in 2013.

He is currently a Research Scientist with the Institute of High-Performance Computing, Agency for Science, Technology and Research, Singapore. His main research interests include soft and continuum robotics modeling and control, multiscale/multiphysics modeling of smart material and hybrid system, nonlinear constitutive modeling and finite element implementation, and process optimization in advanced manufacturing.

Zhuangjian Liu received the Ph.D. degree in engineering from the National University of Singapore (NUS), Singapore, in 2009.

He is currently a Principal Scientist with the Institute of High-Performance Computing, Agency for Science, Technology and Research, Singapore. His main research interests include solid mechanics, numerical simulation, wearable, and flexible electronics soft robotics and sensors.

Dr. Liu was the recipient of the 2018 and 2019 Highly Cited Researchers list from Clarivate Analytics.

Raye Chen-Hua Yeow (Member, IEEE) received the Ph.D. degree in bioengineering from the National University of Singapore (NUS), Singapore, in 2010.

He received postdoctoral training in biorobotics from Harvard University, Cambridge, MA, USA, from 2010 to 2012. He is an Associate Professor and Deputy Head (Outreach & Industry) with the Department of Biomedical Engineering and Advanced Robotics Center, NUS. He is the Program Lead for the Soft and Hybrid Robotics Program under the National Robotics Programme Office in Singapore. He is also currently a Visiting Professor with Computer Science and Artificial Intelligence Laboratory, Massachusetts Institute of Technology, Cambridge, MA, USA. He has authored or coauthored more than 180 journal and conference papers, more than research and innovation awards, and cofounded four soft robotics startups.